

## WEATHERING AND EROSION OF THE POLAR LAYERED DEPOSITS ON MARS; K. E. Herkenhoff, Jet Propulsion Laboratory 183-501, Pasadena, CA 91109

The Martian polar layered deposits are widely believed to be composed of water ice and silicates, but the relative amount of each component is unknown. The "conventional wisdom" among Mars researchers is that the deposits were formed by periodic variations in the deposition of dust and ice caused by climate changes over the last 10 to 100 million years [1]. It is assumed here that water ice is an important constituent of the layered deposits, that the deposits were formed by eolian processes, and that the origin and evolution of the north and south polar deposits were similar.

Calculations of the stability of water ice in the polar regions of Mars [2,3] indicate that ice should not currently be present at the surface of the layered deposits. The present water ice sublimation rate is high enough to erode the entire thickness of the deposits in about a million years. This result suggests that sublimation of water ice from the layered deposits results in concentration of non-volatile material at the surface of the deposits. Such a surface layer would insulate underlying water ice from further sublimation, stabilizing the layered deposits against rapid erosion.

The color and albedo of the layered deposits suggests that bright, red dust is the major non-volatile component of the deposits. However, the differences in albedo and color between mantling dust and exposures of layered deposits in the south polar region [4] and the association of dark dune material with the north polar layered deposits [5] indicates that there is at least a minor component of dark material in the deposits. The dark material may be either sand or dust; each possibility is examined below. The dark material must either be intimately mixed with the bright dust in the layered deposits or occur in layers or lenses less than a few meters in size, or they would be visible in high-resolution Viking Orbiter images.

The presence of small amounts of dark sand in the layered deposits can account for the dark dunes that appear to have sources in the north polar deposits [5]. Poleward circulation during the summer is then required to transport sand into the layered deposits. The most significant problem with this hypothesis is the eolian codeposition of sand and dust in the polar regions. It is unlikely that sand can be carried in suspension by even a much denser Martian atmosphere, so that sand must be transported by saltation [5]. Saltating sand would eject dust into suspension, hindering codeposition of sand and dust. Although small amounts of sand may have saltated over frozen, cemented dust toward the poles, the difficulties with this scenario prompt consideration of alternative hypotheses. A theory for layered deposit formation and evolution involving only dust (bright and dark) and ice is proposed below.

How can dark dust in the layered deposits form the dunes observed in the polar regions? Sublimation of dust/ice mixtures has been shown to result in the formation of filamentary sublimation residue (FSR) particles about 100 microns in size [6]. Such particles can saltate along the Martian surface, and may therefore create dunes [7]. In order to form saltating material by this mechanism that is at least 3 times darker (in red light) than the bright dust that mantles much of Mars, dark dust grains must preferentially form FSR particles. Magnetic dust grains would be expected to form FSR more easily than non-magnetic dust, and are probably much darker. Experimental formation of FSR with magnetic material has not been attempted, and should be the subject of future research.

There is direct evidence for 1-7% magnetic material in the surface fines at the Viking lander sites [8]. In addition, analysis of Viking lander sky brightness data indicates that suspended dust over the landing sites contains about 1% opaque phase, perhaps of the same composition as the magnetic material on the surface [8,9]. Within the uncertainties of these measurements, the percentages of magnetic material given above are identical to the volume of dark dune deposits in the polar regions expressed as a percentage of eroded layered deposits (Table 1). This comparison indicates that the presence of magnetic material in the layered deposits is likely, and that formation of sand dunes from dark FSR particles is plausible.

**WHAT'S WRONG WITH PHOTOCLINOMETRY?** D. G. Jankowski and S. W. Squyres, Department of Astronomy, Cornell University, Ithaca, NY 14853

Topographic data on surface features of planets and satellites are useful in the study of these bodies. Direct measurements of topography are rare. Due to its simplicity and speed, the technique of photogrammetry, which determines surface slopes from brightness variations on spacecraft images, continues to be very popular (1-6). However, photogrammetry will not give reliable results in all cases. Thus it is important that topographic data derived from photogrammetry, like any other data, are not used without associated error estimates.

Photogrammetrically determined slopes contain errors from the following sources:

- i. Image noise: Image noise is a source of error because it produces spurious intensity fluctuations from pixel to pixel.
- ii. Digitization: The digitization of brightness levels in all spacecraft images results in an inherent slope uncertainty.
- iii. Background: An incorrect dark current will introduce systematic errors.
- iv. Photometric function uncertainties: An improper photometric function is obviously a source of error.
- v. Albedo errors: The surface albedo can be a source of error both due to uncertainties in the mean regional albedo (often assumed constant) and due to albedo variations.
- vi. Atmospheric effects: An atmosphere can be a source of error due both to uncertainties in the mean contribution of light scattered and due to fluctuations of this contribution across the image.
- vii. Scanline misalignment: Most photogrammetry techniques are one-dimensional, determining the topography only along a specified line. Such techniques are typically restricted to scanlines that travel directly up or down all slopes. Hence slope errors can also occur due to the misalignment of scanlines.
- viii. Viewing and lighting geometry uncertainties: The errors associated with viewing and lighting geometry uncertainties associated with recent spacecraft are for the most part insignificant compared to other errors, and will not be discussed.

We have performed an investigation of the quantitative effect of each of these error sources on the photogrammetric method. The error contributions due to the above sources are modelled under conditions appropriate for spacecraft images of Ganymede and Mars. The characteristics of Viking Orbiter images are used for modelling Mars and the characteristics of Voyager images are used for Ganymede. The noise characteristics of the Galileo camera are included as a comparison with the Voyager cameras. The Lommel-Seeliger photometric function is used to model grooved terrain on Ganymede (1), and the Minnaert function is used to model the surface of Mars (5).

Photogrammetric slope uncertainties due to the above sources have been plotted on photometric latitude-longitude grids for phase angles of  $30^\circ$ ,  $60^\circ$ , and  $90^\circ$ . Slope errors are investigated for "actual" slopes of  $0^\circ$ ,  $10^\circ$  (sloping away from the sun), and  $-10^\circ$  (sloping towards the sun). Slope errors are also investigated for rotation angles (the angle subtended by the scanline direction and the local photometric latitude line) ranging from  $30^\circ$  to  $-30^\circ$ .

At small incidence angles, the photometric functions change very slowly; thus small brightness variations in this region correspond to large topographic slopes. Hence the effects of albedo variations, atmospheric variations, noise, and digitization are all enhanced near the subsolar point. This is clearly seen in Figures 1a and 1b, which show contours of the slope error due to a 5% albedo variation on Mars and Ganymede, respectively. The errors in Figure 1 were calculated for a point with  $0^\circ$  slope along a scanline with a rotation angle of  $0^\circ$ . The phase angle is  $60^\circ$ . Albedo variations are inevitably a significant error source in photogrammetry.

The noise levels characteristic of the Viking and Voyager cameras result in significant slope errors at low incidence angles. The errors associated with Viking images are the largest, near  $2^\circ$  at the subspacecraft point at  $60^\circ$  phase. The errors associated with the Galileo camera are still uncertain, primarily due to uncertainties in the effects of the harsh radiation environment. Using noise values characteristic of the CCD detector suggests that the slope error attributable to Galileo noise will be essentially negligible. For all images considered, errors associated with digitization and incorrect dark currents are negligible compared to noise errors.

In summary, weathering of the layered deposits by sublimation of water ice can account for the geologic relationships observed in the polar regions. The non-volatile component of the layered deposits appears to consist mainly of bright red dust, with small amounts of dark dust or sand. Dark dust, perhaps similar to the magnetic material found at the Viking Lander sites, may preferentially form filamentary residue particles upon weathering of the deposits. Once eroded, these particles may saltate to form the dark dunes found in both polar regions. Eventual destruction of the particles could allow recycling of the dark dust into the layered deposits via atmospheric suspension. This scenario for the origin and evolution of the layered deposits is consistent with the available data.

## REFERENCES

- [1] Carr, M. H. (1982). *Icarus* **50**, 129-139.  
 [2] Toon, O. B., J. B. Pollack, W. Ward, J. A. Burns, and K. Bilski (1980). *Icarus* **44**, 552-607.  
 [3] Hofstadter, M. D. and B. C. Murray (1990). *Icarus*, in press.  
 [4] Herkenhoff, K. E. and B. C. Murray (1990). *J. Geophys. Res.*, in press (Mars polar processes issue).  
 [5] Thomas, P. C. and C. Weitz (1989). *Icarus* **81**, 185-215.  
 [6] Storrs, A. D., F. P. Fanale, R. S. Saunders, and J. B. Stephens (1988). *Icarus* **76**, 493-512.  
 [7] Saunders, R. S., T. J. Parker, J. B. Stephens, E. G. Laue, and F. P. Fanale (1985). *NASA Tech. Mem.* **87563**, 300-302.  
 [8] Hargraves, R. B., D. W. Collinson, R. E. Arvidson, and P. M. Cates (1979). *J. Geophys. Res.* **84**, 8379-8384.  
 [9] Pollack, J. B., D. Colburn, F. M. Flasar, R. Kahn, C. Carlston, and D. Pidek (1979). *J. Geophys. Res.* **84**, 4479-4496.  
 [10] Thomas, P. (1982). *J. Geophys. Res.* **87**, 9999-10008.

Table 1

| Quantity   | Fraction | Reference |
|--|----------|-----------|
| Magnetic material in surface fines                   | 1-7 %    | [8]       |
| Opaque phase in atmospheric dust                     | 1 %      | [9]       |
| Volume of dark dunes/volume of eroded polar deposits | 1-10 %   | [10]      |

The Martian atmosphere clearly can not be ignored when doing photoclinoetry. However, with the help of resolved shadows (5), the contribution of the atmosphere can be estimated fairly well in many Viking images. The atmospheric contribution can often be estimated with less than 10% error. Fluctuations within a given image are small, usually much less than 5%. The errors associated with these uncertainties are less than 1°.

Errors due to uncertainties in the Minnaert K parameter are generally not larger than 1°. However, for large slopes and large rotation angles, this error source can become much more significant, even at large incidence angles, where other errors sources disappear.

Errors due to misalignment can be significant if the misalignment angle is larger than about 10°. The errors tend to be larger for the Minnaert function than for the Lommel-Seeliger function, and they tend to be smaller for lower rotation angles (scanline directions chosen parallel to lines of photometric latitude) for both functions. For the Minnaert function, scanlines directions chosen parallel to lines of photometric latitude) for both functions. For the Minnaert function, scanlines pointing away from the sun are more accurate when pointing away from the photometric equator at a given angle than when pointing towards the equator at the same angle.

Slope errors are usually larger for sun-facing slopes than for slopes facing away from the sun. This effect is generally stronger for the Lommel-Seeliger photometric function than it is for the Minnaert function. The errors associated with uncertainties in the Minnaert K parameter and with scanline misalignment both increase significantly with increasing slope.

Slope errors decrease with increasing phase angle. The optimal phase angle for photoclinoetry is about 60°. Smaller phase angles result in larger errors, while larger phase angles result in smaller adequate surface areas and larger geometric foreshortening.

Slopes determined using photoclinoetry contain errors from a number of different sources. The size of the error varies significantly depending upon the imaging system used, the lighting and viewing geometry, and the nature of the surface imaged. Hence, photoclinoetry codes should always include error estimates with each topographic profile to help determine their reliability.

**References:** (1) Squyres, S. (1981) *Icarus* **46** 156-168. (2) Davis, P., Soderblom, L. (1984) *J. Geophys. Res* **89** 9449-9457. (3) Moore, J., McEwen, A., Albin, E., Greeley, R. (1986) *Icarus* **67** 181-183 (4) Jankowski, D., Squyres, S., (1988) *Science* **241** 1322-1325. (5) Tanaka, K., Davis, P. (1988) *J. Geophys. Res* **93** 14893-14917. (6) Schenk, P. (1989) *J. Geophys. Res* **94** 3813-3832.

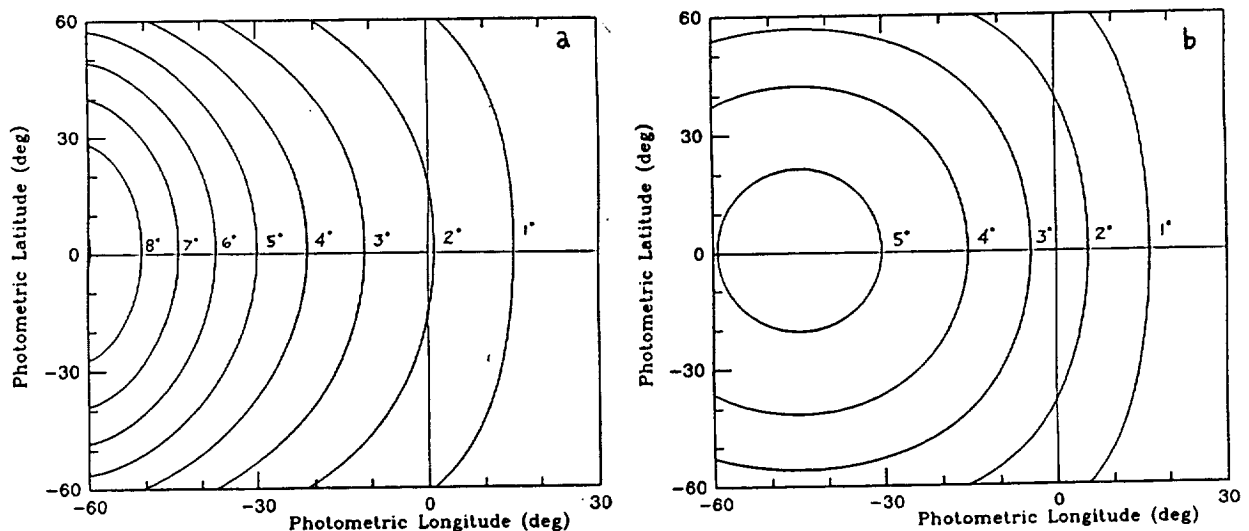


**Figure 1.** a) Contours of slope errors due to a 5% albedo error on Mars. b) Contours of slope errors due to a 5% albedo error on Ganymede.

FURTHER EVIDENCES FOR HORIZONTAL BLOCK-/PLATE MOVEMENTS AND/OR NAPPE TECTONICS WITHIN THE  
TANOVA - UPDOMING AND ALONG ITS MARGIN, MARS

Heinz - Peter Jöns, Geologisches Institut der T.U. Clausthal; Leibnizstrasse 10; 3392 Clausthal-Zellerfeld; F.R.Germany

Earlier investigations of the relief of the martian uplands led to the discovery of an old volcanic province south of the Tharsis-dome and the Claritas Fossae (1). Additional detailed investigations of the relief of the entire area of the martian uplands led to the discovery of the existence of at least about one more dozen very old unclassified volcanoes (shield- or stratovolcanoes?) which are situated exclusively within the oldest parts of the martian uplands. These volcanic edifices are predominantly arranged along ancient linear or curvilinear zones of weakness. The spatial distribution of these very old volcanoes is of special interest and allows the identification of four groups:

- ) The first group which has been described as new volcanic province is clustered along arcuate zones of weakness east and west of the Claritas Fossae and is arranged concentrically with respect to the Noctis Labyrinthus-dome.
- ) The second group consists of volcanoes which are clustered along very old linear features (grabens?).
- ) The third group is probably impact-related, because these features are situated along concentric features in the vicinity of Hellas and probably in the vicinity of Isidis as well.
- ) The remaining volcanoes of this type seem to occur with a random distribution in the oldest parts of the martian uplands. A relation of these structures to any tectonic feature(s) is so far not detectable (2).

Detailed studies of the area which contains these volcanoes led to the conclusion that block movements and/or nappe tectonics have happened in the early martian history which led to the formation of an arcuate zone of collisional features in the surrounding of the TaNoVa-updoming (3, 9). The most important and most obvious hints for the existence of a probable zone of collision east of the Claritas Fossae is indicated by:

- a) subparallel compressional features (narrow ridges),
  - b) rows of so called flat irons,
  - c) features of overthrusting (nappe tectonics),
  - d) and a cuesta landscape which runs parallel to the latter features (Fig. 1).
- All these features are arranged concentrically with respect to Syria Planum. They form a belt which is appr. 100 - 200km wide.

As the boundary of the TaNoVa-Updoming is clearly indicated along its eastern and southern margin between the Valles Marineris and the Claritas Fossae (sector A) it is a task which suggests itself to look for similar features along its western margin within sector B. Although the western boundary is less clearly indicated by the relief it is noteworthy that the same set of features with the same spatial distribution which is typical for sector A can be detected between  $-30^{\circ}$  and  $-55^{\circ}$  lat. and between  $160^{\circ}$  and  $190^{\circ}$  long. as well:

- a) arranged concentrically with respect to Arsia Mons/Syria Planum wrinkle ridges,
- b) arranged concentrically compressional ridges together with series of so called flat irons and probable thrust fronts,
- c) a prominent radial shear zone which has cut and reshaped a large mountain into a unique set of lamellar ridges,
- d) rows of very old unclassified volcanoes (4),
- e) many compressed impact structures the longer axis of which runs tangential with respect to the margin of the TaNoVa-updoming within sector B, (Fig. 2).

It is noteworthy that the large impact basin Orcus Patera which is situated along the northern continuation of this area is highly deformed as well with the same orientation of its longer axis (5).

Due to the spatial distribution of the described features (c o n c e n t r i c a l l y with respect to Syria Planum, the most elevated area of the TaNoVa-updoming with a maximum elevation of about 10 000m) the supposition seems to be justified that the whole set of concentric features can be interpreted as a fossil embryonic mountain range which probably indicates plate and/or block tectonics together with younger nappe tectonics along the border of the southern half of the TaNoVa-updoming.

The distribution of large-scale radial features reveals additional hints for block/plate margins in that area. The young (recent?) volcanism in the Valles Marineris (6) could indicate a probably still active spreading axis. A similar type of endogenic activity is imaginable with respect to the origin of Alba Patera and its remarkable rift-like features (7). If this hypothesis is right it seems to be an obvious conclusion that the northern branch of the Kasei Valles may be interpreted as indicating an axis of descending material (8). In this context it should be pointed out that Tharsis Tholus which is situated exactly on the southwest extension of the northern branches of the Kasei Valles is the only martian volcano which has been cut and sheared along linear features. Hence, intensive tectonic stresses must have acted along that axis. The Claritas Fossae which are the boundary between sector A and B of the TaNoVa-updoming remain a mystery. But the ancient volcanoes along the southern part of that prominent linear structure justify the supposition that this feature indicates a block boundary as well (Fi. 3).

#### References

- 1) Scott, D.H. and Tanaka, K.L. (1981), Proceedings of the XIIth Lun. and Plan. Sci. Conf., 1449 - 1458.
- 2) Jöns, H. - P. (1990), The Mars, Global Map of Mars, in press.
- 3) Jöns, H. - P. (1982), ESA SP - 185, (Proceedings), 89 - 105.
- 4) Scott, D.H. and Tanaka, K.L. (1986), Geologic Map of the Western and Equatorial Region of Mars, U.S.G.S., I - 1802-A.
- 5) Jöns, H. - P. (1984), Lun. and Plan. Sci. XV, Abstracts, Part 1, 415 - 416.
- 6) Lucchitta, B.K. (1985), Lun. and Plan. Sci. XVI, Abstracts, Part 2, 503 - 504.
- 7) Raitala, J. (1988), Earth, Moon, and Planets 42, 277 - 291.
- 8) Jöns, H. - P. (1989), Lun. and Plan. Sci. XX, Abstracts, Part 2, 486 - 487.
- 9) Jöns, H. - P. (1989), Lun. and Plan. Sci. XX, Abstracts, Part 2; 484 - 485.

LEGEND (Fig.3)

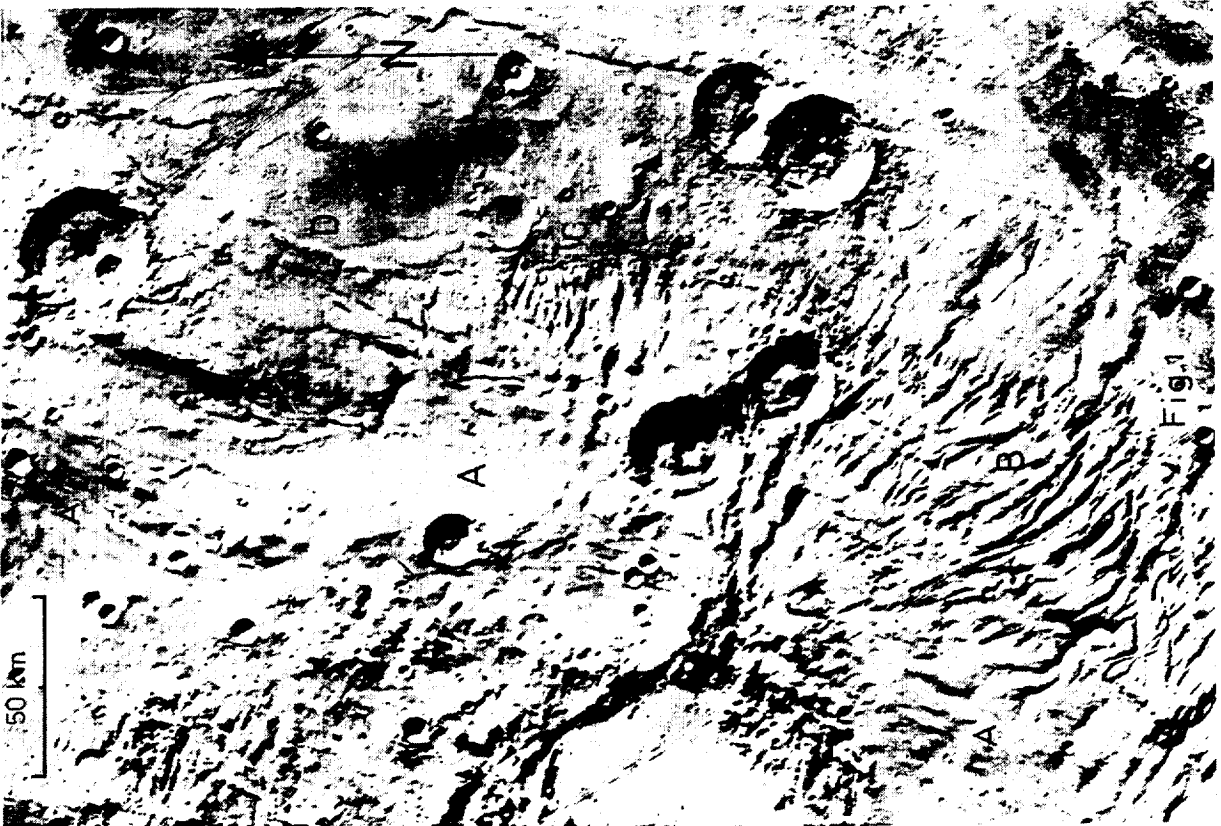
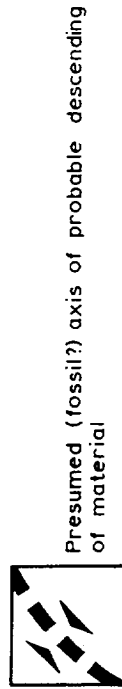
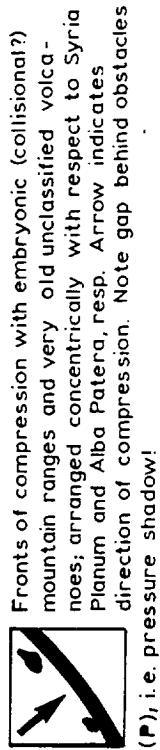
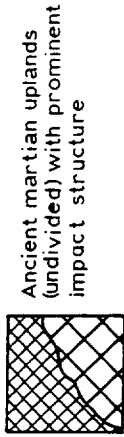
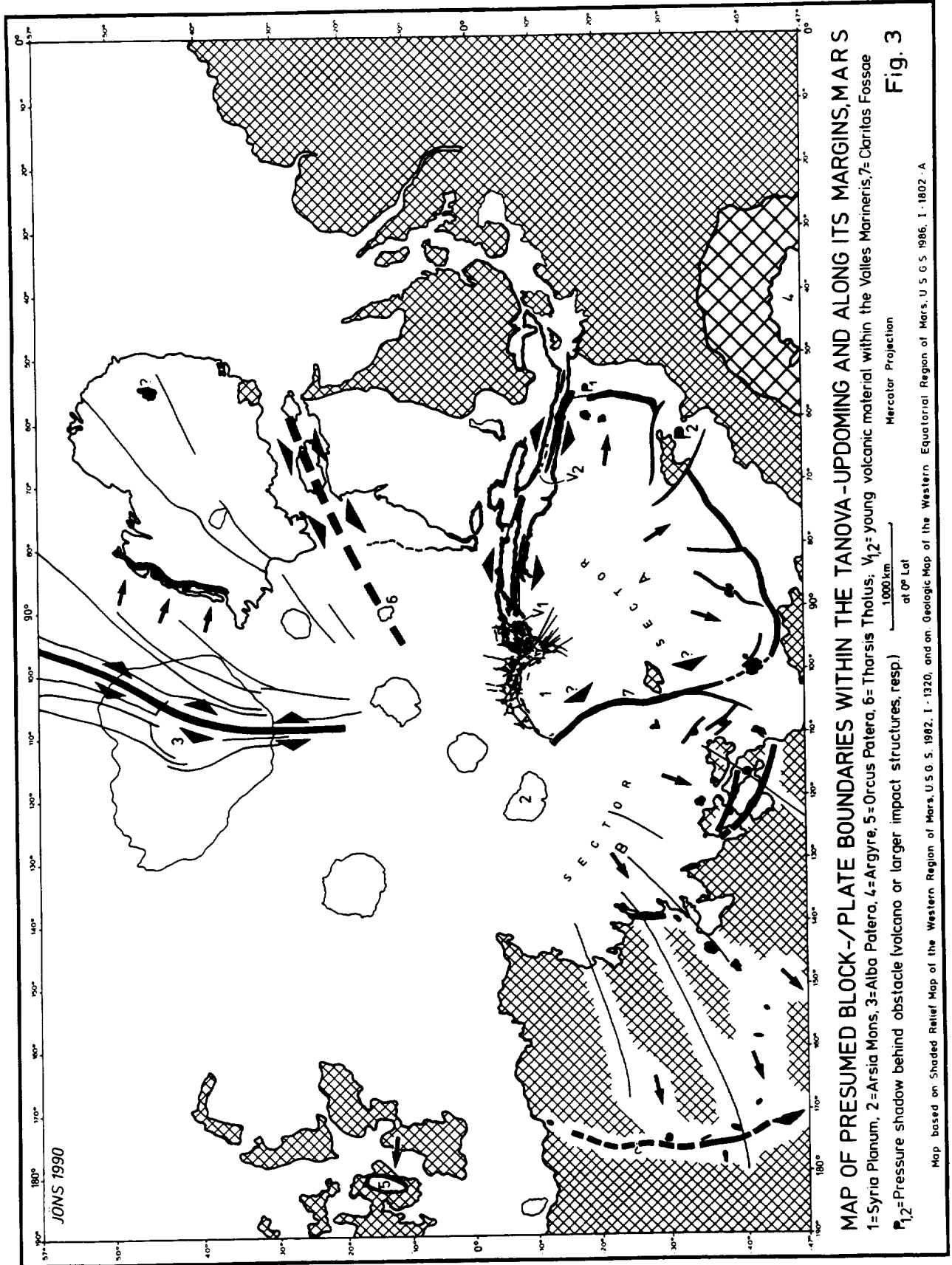


Fig. 1  
 Eastern margin of the TaNoVa - Updoming in sector A:  
 Compressional ridges (A); rows of so called flat  
 irons (B); cuesta landscape (C); and front of over-  
 thrust material (D).



Western margin of the TaNoVa - Updoming in sector B: Thrust front (arrow 1); vergency of wrinkle ridges, same vergency as in the case of the thrust front! (arrow 2); rows of so called flat irons (arrow 3); subparallel compressional ridges (arrow 4); and sheared mountain with lamellar ridges (5).



THE PLANET MARS: PRESENTATION OF A GLOBAL MAP

Heinz - Peter Jöns, Geologisches Institut der T.U. Clausthal; Leibnizstrasse 10; 3392 Clausthal - Zellerfeld; F.R. Germany

A global map of Mars will be presented at a scale of 1:30 Mill. with the projection of HAMMER'S equal area planisphere. Four main sets of morphologic units have been outlined on this map - beside the most prominent impact structures Argyre, Isidis, and Hellas which form units of its own:

- 1) The ancient martian uplands (predominantly southern hemisphere),
- 2) the updomings of Tharsis, Noctis Labyrinthus, and Valles Marineris (= TaNoVa), and Elysium,
- 3) the lowlands of Mars (predominantly northern hemisphere), and
- 4) the polar caps.

The main purpose of this map is to demonstrate the relief genesis, the relief dynamics, and (as a result of both) the now existing relief division. It is obvious that the bulk of activities which reshaped the planets primitive relief has happened in the area of the TaNoVa - and the Elysium - updomings and along their margins.

Large - scale depressions which occupy the centre of the TaNoVa - updoming have been interpreted as a result of melting of permafrost and/or ground ice which led to the origin of giant progressive chaotic terrains. During their activity these features delivered their mobilized material (mud, aqueous slurry, debris, water) into the already existing circum-polar depression of the northern hemisphere of Mars which led to the origin of some generations of fossil (mud) oceans in that area (1).

A reactivation (or simply continuation?) of the Tharsis (and Elysium?) volcanism resulted in a large - scale flooding of the adjacent permafrost - related depressions (meltplains) with younger lavas. But remnants of these meltplains have been preserved along the border of the Tharsis - updoming (arcuate escarpments and a set of special morphologic features northwest of Olympus Mons). Smaller (catastrophic?) outflow events happened into the Chryse Planitia, within Isidis Planitia, probably into Hellas Planitia, and in the vicinity of the South Pole and from that area into Argyre Planitia (2). The youngest fossil (mud) ocean within the lowlands of the northern hemisphere was probably the result of polar basal melting (3).

The general border of the TaNoVa - updoming south of the equator is indicated by a special set of morphologic features (wrinkle ridges, zones of compression, rows of so called flat irons, a cuesta landscape, and numerous very old unclassified relatively small volcanoes) which are mainly arranged concentrically with respect to Syria Planum, the most elevated area of the TaNoVa - updoming. That set of features -together with the much younger giant shield volcanoes and the large linear tectonic features to which they are closely related- offers the possibility to identify areas of nappe tectonics (mainly together with concentrically arranged features) as well as (fossil?) embryonic block/plate boundaries (mainly with radially arranged linear features), (4).

This global map will show for the first time the dynamic events and their results described above together with many other important features of the planet's entire surface. The map will be printed at the Lithographisches Institut, Potsdamer Str. 91, Berlin, F.R.Germany; it will be available from August 1990 from that institute.

References

- 1) Jöns, H. - P. (1990), Geologische Rundschau, 79/1, 131 - 164.
- 2) Jöns, H. - P. (1987), Lun. and Plan. Sci. XVIII, Abstracts, Vol.2, 470 - 471.
- 3) Clifford, S.M. (1987), J. of Geophys. Res., 92, No, 89, 9135 - 9152.
- 4) U.S. Geological Survey (1979 - 1985), Atlas of Mars, 1:2 Mill. Topographic Series, 140 sheets of the "Controlled Photomosaic" - version.

SCIENTIFIC AND ENGINEERING APPLICATIONS OF THE MARS-GLOBAL REFERENCE  
ATMOSPHERIC MODEL (MARS-GRAM): Justus, C.G. and James, Bonnie

Results and applications for a new model of the Martian atmosphere are discussed. The Mars Global Reference Atmospheric Model (Mars-GRAM) is based on parameterizations to approximate, as realistically as possible, the temperature, pressure, density and winds of the Martian atmosphere, and their latitudinal, longitudinal, diurnal, seasonal and altitude variation, from the surface through thermospheric altitudes. Parameterizations are also included for the effects of global-scale dust storms on the variations of the thermodynamic and wind properties of the Martian atmosphere. Mars-GRAM is written in Fortran 77, and is designed to run on an IBM-PC or compatible microcomputer. With the planned addition of radiation budget parameterizations, Mars-GRAM will have a variety of possible scientific applications as a "poor man's global circulation model" for the atmosphere of Mars. Among these are: (1) an ability to provide realistic, geographically and seasonally-dependent backgrounds of temperature and wind for studies of tides and atmospheric propagation of other wave disturbances (e.g. gravity waves, mountain lee waves, etc.); (2) similar background fields of temperature and pressure for other environmentally varying physical processes (e.g. cloud nucleation process models, temperature-dependent chemical rate models, etc.); (3) studies of surface radiation budget, boundary layer dynamics, and synoptic and global-scale dynamics; and (4) investigations of the surface-atmosphere flux of dust and the zonal and meridional transport of dust during local-scale and global-scale dust storms. In addition, a number of mission-oriented engineering applications are envisioned for Mars-GRAM (e.g. aerocapture mission profile studies, Mars Rover Sample Return mission planning and design studies, Mars 94 balloon heating loads and trajectory studies, etc.). Figures 1-4 show samples of the output which can be produced by the Mars-GRAM program.

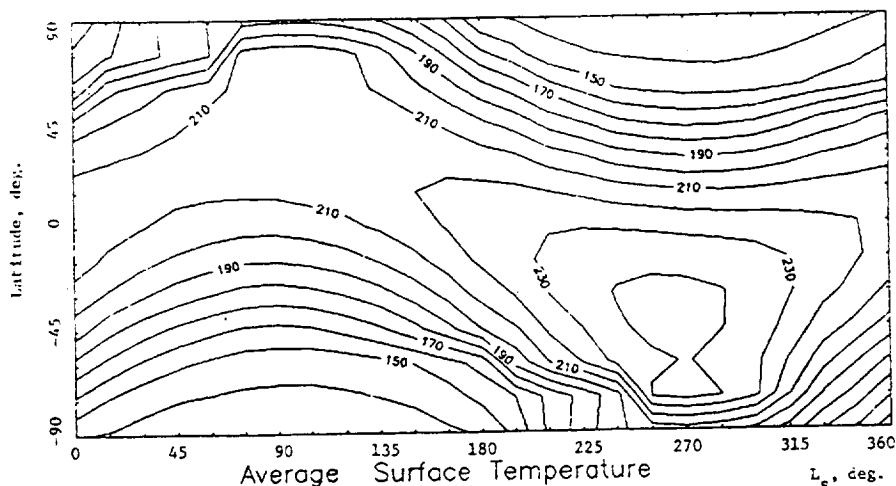


Figure 1 - Seasonal and latitudinal variation of daily average surface temperature, computed by the Mars-GRAM model.  $L_s$  is the areocentric longitude of the sun.

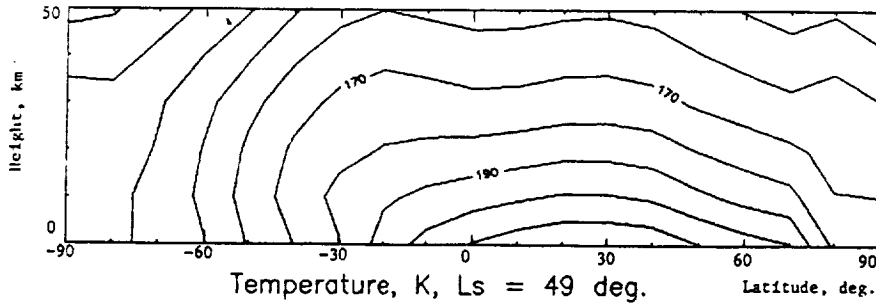


Figure 2a - Cross section of temperature (K) at 9 am local time for  $L_s = 49^\circ$ .

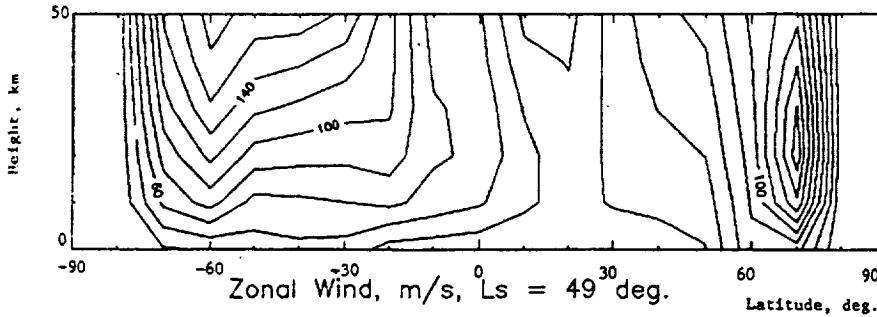


Figure 2b - Cross section of zonal wind (m/s) at 9 am local time for  $L_s = 49^\circ$ .

Figure 3 - Progression of simulated dust-storm effect on daily average, maximum and minimum temperature versus latitude and  $L_s$  value (degrees) for the 1977b storm.

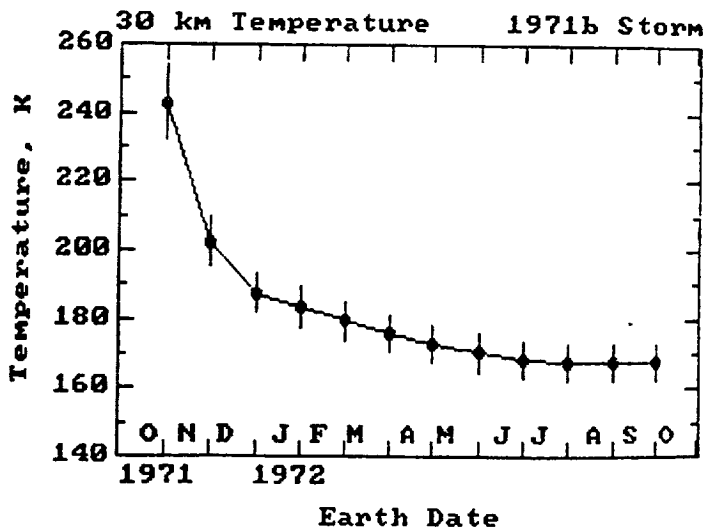
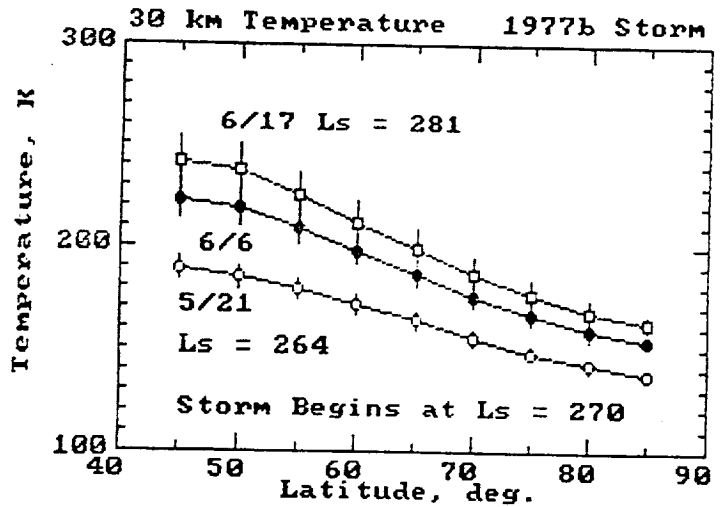


Figure 4 - Progression of simulated dust-storm effect on daily average, maximum and minimum temperature versus time at latitude at  $25^\circ S$  for the 1971b storm.

**Ancient Glaciation on Mars** J.S. Kargel and R.G. Strom, Lunar and Planetary Laboratory, University of Arizona, Tucson, AZ 85721

Photogeologic evidence for widespread ancient episodes of glaciation has been discovered in Viking spacecraft images of Mars. The principal image base used for this study consists of the USGS 1:2 million scale photomosaics of the MC-26 Quadrangle and the Viking Orbiter images obtained on orbits 349S, 352S, 567B, 568B, 569B, and 574A. We recognize that non-glacial mechanisms may adequately explain certain individual types of landforms discussed below. However, we believe that a glacial hypothesis provides a more acceptable unified explanation, and is consistent with the emerging outlines of a global hydrologic model [1].

Figure 1 is a glaciological map of a region the Charitum Montes and the adjoining Argyre Planitia. The most startling feature in this region is an anastomosing system of sinuous ridges, noted previously [2-5]. The plan of this ridge system (Viking Orbiter frames 352S34 and 567B30-35) is fluvial in character and must therefore have an underlying fluvial explanation (volcano-tectonic processes can not generate this pattern). The possibility that similar ridge systems elsewhere on Mars are glacial eskers has been previously noted [2] (eskers are stream deposits of sand and gravel originally laid down on the surface of, within, or beneath stagnant, melting glaciers). The esker hypothesis is lent support by the similarity in length, height, width, overall structural plan, and detailed structure of the Martian features compared to large terrestrial eskers associated with the melting of Late Pleistocene and modern ice sheets on Earth [6, 7].

Figure 1 also shows the characteristic structure of the mountainous inner ring of Argyre, including numerous valleys separating sharp linear to semi-circular ridges. The characteristics of this mountain range, if considered with a terrestrial perspective, are diagnostic of alpine-type glacial erosion. The Charitum Montes appear to be a classic glacial assemblage of horns, cirques, and aretes, with intervening valleys mantled by lobate debris aprons. A prominent cirque near 54°30'S. Lat. 31°30'Long. is intimately associated with a region of fluvial deposition and erosion interpreted to be a glacial outwash deposit (sandur plain). Another region of fluvial erosion and deposition, near 54° S. Lat. 37° Long., emanates from a large glacially modified valley in the Charitum Montes and is interpreted as a glacio-lacustrine delta.

Large-scale glacial fluting was severe in Argyre Planitia during the height of the ancient ice age. The scouring of several large impact crater rims (e.g., frame 568B33) demonstrates that a considerable interval of time elapsed between the Argyre impact and the glacial epoch. In the area mapped in Figure 1 (450,000 km<sup>2</sup>) there are seven fresh impact craters larger than 10 km in diameter displaying fresh ejecta and sharp rims and lacking any signs of glaciation, suggesting an early Amazonian termination of the glacial epoch. The extensive ejecta blanket of the large crater Galle (not one of the seven) covers about a third of Argyre Planitia, and clearly mantles many glacial grooves and ridges (e.g., frame 352S39). However, the delta-like fluvial system mentioned above erodes and elsewhere embays the ejecta blanket of Galle; further, smooth layered deposits, interpreted as glacio-lacustrine sediments associated with the esker system, embay Galle's ejecta blanket (frames 567B36 and 568B09); finally, a channel, either glacial or possibly fluvio-glacial, incises the rim of Galle (frame 352S24). Hence, Galle dates from the glacial epoch (or an interglacial). Impact into an ice sheet is suggested by the extensive occurrence of ice disintegration features (e.g., kettle holes) on the ejecta blanket of Galle (frame 568B12). Possibly an underlying ice sheet, or perhaps anomalously large quantities of ice entrained in the ejecta itself, later melted or sublimated.

Kettle fields outside the area of Galle's ejecta testify to the retreat of the ice sheet and the stranding of large blocks of ice on Argyre Planitia (frame 568B53). Together with the eskers and outwash deposits these landforms record the melting of the Argyre ice sheet, *indicating a period of relatively warm climate even at moderately high elevations and latitudes*. However, the absence of super-imposed fluvial systems (other than those plausibly related to the melting of ice) indicates that *humid conditions following the ablation of the ice sheet were short-lived*. We note that the northern rim escarpment of Argyre has been fluvially modified and lacks evidence of glaciation, as if it rained there probably at the time that it snowed at higher latitudes.

We have made a preliminary search for possible glaciogenic landforms elsewhere on Mars. The single most diagnostic glaciogenic landform on Mars probably is the esker. Eskers are widespread in the Southern Hemisphere of Mars, often occurring in close association with polar layered deposits and etched (kettled and/or glacially scoured?) terrains; these probably indicate that a vast ice sheet once enveloped much of the Southern Hemisphere down to about 40° S. Lat. Eskers also occur more sparingly in the Northern Lowlands north of 26° in close association with the "thumbprint terrains" (recessional moraine fields?), and in one tropical location.

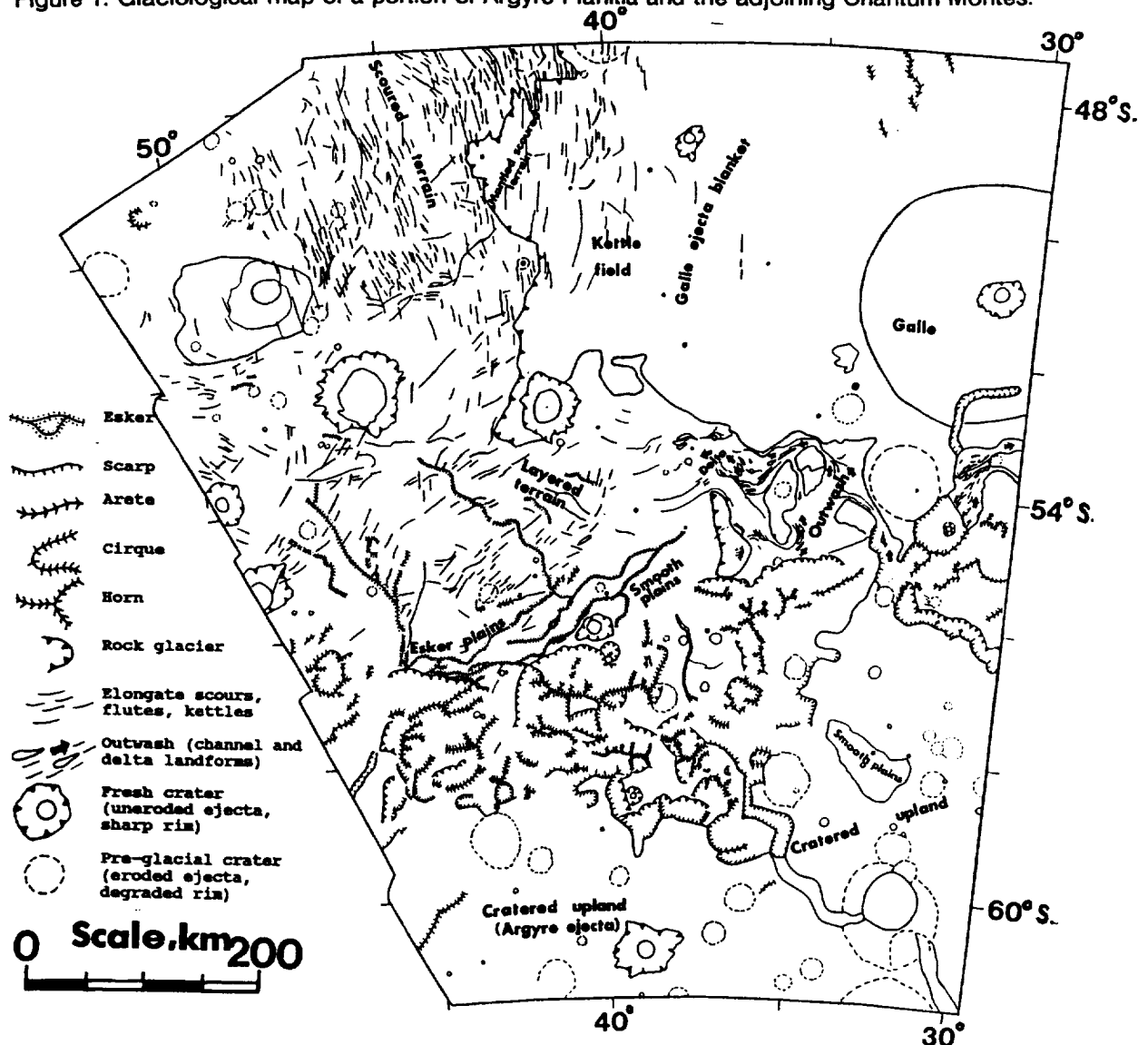
The final ablation of the southern ice sheet must have occurred under much warmer conditions and under a denser atmosphere than currently prevail. Glaciation and de-glaciation may have been two steps

In a global hydrologic cycle. Possibly Oceanus Borealis [1] supplied the atmosphere with water vapor which then was cold-trapped as snow or frost in the high elevations of the Southern Hemisphere. As the climate warmed due to climatic perturbations related to the formation of Oceanus Borealis the ice sheet eventually melted, charging the cratered uplands with groundwater. Given sufficient permeability this groundwater may have flowed northward to re-charge the equatorial region. Volcanism-driven outbursts of groundwaters may have re-filled Oceanus Borealis, completing the cycle, possibly on a repeating basis [8, 9].

Finally, we suggest that the nature and significance of the lobate debris aprons at high- and mid-latitudes on Mars [10] should be re-evaluated. It is generally thought that these debris aprons are rock glaciers. The outstanding issue is whether they are purely periglacial rock glaciers where down-slope motion is generated by gelifluccion (surficial freeze-thaw), or whether the debris aprons are ice-cored rock glaciers where a rocky lag has accumulated on the surfaces of old glaciers by processes of melting and/or sublimation [11]. Figure 1 shows that debris aprons are commonly associated with individual cirques, suggesting a glacial origin.

References. 1) V. Baker et al., 1990, *LPS XX*. 2) M.H. Carr et al., 1980, *Viking Orbiter Views of Mars*, U.S. Gov't. Printing Office, Washington, D.C., p. 136. 3) P.H. Schultz and D. Britt, 1986, *LPS XVII*, p.775. 4) T.J. Parker, 1989, *LPS XX*, p. 826. 5) C.A. Hodges, 1980, Geologic Map of the Argyre Quadrangle of Mars, USGS Map I-1181. 6) R.J. Price, 1973, *Glacial and Fluvio-glacial Landforms*, Oliver & Boyd, Edinburgh, 242 pages. 7) H. Lee, 1965, *Geol. Surv. Can. Pap.* 65-14, 1-17. 8) V. Gulick and V. Baker, 1990, *LPS XXI*. 9) G. Komatsu and R.G. Strom, 1990, *LPS XXI*. 10) S.W. Squyres and M.H. Carr, 1986, *Science* 231, 249-252. 11) J.R. Giardino, J.F. Schroder, Jr., and J.D. Vitek (eds.), 1987, *Rock Glaciers*, Allen & Unwin, Boston, 355 pages.

Figure 1. Glaciological map of a portion of Argyre Planitia and the adjoining Charitum Montes.



**POST-FLOODING MODIFICATIONS TO CHRYSE BASIN CHANNELS, MARS:  
IMPLICATIONS FOR SOURCE VOLUMES AND EVOLUTION OF THE CHANNELS**  
R. Craig Kochel, Department of Geology, Bucknell University, Lewisburg, PA 17837 and  
Jerry R. Miller, Quaternary Sciences Center, Desert Research Institute, Reno, NV 89506

The mid-latitude Chryse Planitia basin on Mars is host to a complex of large-scale outflow channels along its southern margin. The Chryse channels have been interpreted by most investigators as the erosional product of catastrophic floods which emanated from equatorial source regions characterized by chaotic terrain. Foremost among the unresolved questions concerning channel evolution is an apparent disparity between the volumes of the proposed source areas and downstream channel reaches. In addition, there has been considerable speculation regarding mechanisms which have the ability to release water at rates and volumes consistent with the large-scale flooding dictated by the interpretation of erosional and depositional landforms within the channels. Most source areas have exceedingly small volumes compared to the estimates of discharges required to produce their downstream geomorphology.

Systematic interpretation and mapping of margins along the Chryse outflow channels indicates that degradation of channel walls and floors has been significant. Post-channeling volume enlargement of downstream channel reaches has significant implications regarding the estimates of discharges required in their formation. Post-channeling modification appears to have been dominated by rockfall, debris-flow, slumping, and groundwater sapping processes. The importance of these modification processes varies spatially along individual channels and between systems. These patterns may provide important clues to variations in the composition of host terrains or regional geothermal conditions in the Martian regolith.

Deeply incised channels such as Kasei Vallis have undergone the most extensive post-channeling enlargement, while less incised systems like Maja Vallis exhibit present channel dimensions likely to be very close to their original character. The variation in geomorphic style and degree of incision of the Chryse outflow channels may have important implications regarding formative processes and sources of water. Kasei Vallis is the most deeply incised channel system, with escarpment heights of 2 - 3 km common between its channel floor and the host terrain surface of Lunae Planum. The extreme incision and concomitant large volume of Kasei Vallis may not all be attributable to flood erosion. Schumm (1974) suggested that Kasei Vallis may be a structural landform associated with extension related to the Tharsis Uplift west of the channel. Orientations of geomorphic features within the Kasei channel conform with the trends of regional structural features in the area (Kochel and Burgess 1983, Chapman and Scott 1989), providing support for the suggestion that the Kasei Vallis floods may have used and modified a preexisting structural trough similar to Valles Marineris. This would help explain the anomalous depths of the channel compared to others along the Chryse basin margin.

The disparity between source area and channel volumes varies significantly between individual channel systems. The disparity is greatest for Kasei Vallis and its assumed Echus Chasma source and least for Maja Valles and its Juventae Chasma head. The proximity of upstream segments of Kasei Vallis to the Tharsis volcanic complex presents another possible mechanism for explaining the exaggerated development of the Kasei channel system and apparent insignificance of Echus Chasma to supply needed the volumes of outflow necessary to erode the channel. Geothermal heating emanating from early stages of Tharsis volcanic activity could have produced diffuse but widespread regional thermal degradation of the western portions of Lunae Planum. Water released from the formerly frozen regolith would likely have ponded in large lakes upstream from the incised reaches of Kasei Vallis (upstream of the major eastward bend in the channel). Once lake levels overtopped the divide

catastrophic flooding could have ensued down the structural trough of Kasei Vallis. It is likely that numerous floods would have occurred as ice dams may have formed and failed repeatedly as the degradation of Lunae Planum continued along its western margin. This proposed scenario suggests that flows emanating from Echus Chasma played a minor role in the erosion of the Kasei Vallis complex compared to water originating from more diffuse sources downstream.

In contrast to Kasei Vallis, Maja Vallis exhibits much less incision into the host rocks of Lunae Planum and has substantially less disparity between potential source flows and channel volumes. The increased distance from the Tharsis volcanic center may have precluded wholesale degradation of ground ice in Lunae Planum beyond the present location of its westernmost escarpment (approximately 73° W longitude). The style of channel margin degradational features subsequent to channeling along Kasei Vallis appear to change systematically across this longitudinal zone; thus, providing support for this interpretation. East of the Kasei region, potential channel sources related to geothermal processes were probably limited to more localized intrusive activity of the scale represented by the chaos in the Juventae Chasma source area for Maja Vallis. Geomorphic evidence of multiple flow events (DeHon 1989, Baker and Kochel 1979) in downstream reaches of Maja Vallis and associated overflow channels to the north indicate that there is little disparity between source and channel volumes for this system. Similar arguments may be made for the development of Shalbatana Vallis along the southern Chryse margin.

The complex of channels (notably Ares, Tiu, and Simud Vallis) along the southeastern margin of Chryse basin exhibit incision into their host terrain intermediate between Kasei and Maja Vallis. Evidence of structural control is lacking, indicating that the incision is entirely due to flood erosion and will have to be accounted for in consideration of the evolution of these channel systems. Detailed geomorphic studies of this region by Grant (1987) showed that channel evolution was exceedingly complex and involved numerous flood events from multiple sources. Zones of chaos occur at numerous locations within the upper reaches of the channels. Their morphology indicates that the channel systems developed by progressively extending their head regions southward toward Valles Marineris with successive appearance of source chaos areas. As the channels grew, the most recent flows eroded downstream chaos regions. Eventually, headward extension breached the divide and allowed ponded water within eastern Valles Marineris to empty catastrophically into the channels. The combination of flow events is likely to be great enough to explain the substantial downstream volume of material eroded to form these channels. Whether the mechanism for release of water to these source areas is related to localized intrusions or associated with the failure of overpressured aquifers (Carr, 1979) is unclear.

Given the scenario of events suggested above to explain the flood flows for the Chryse basin outflow channels in combination with channel volumes adjusted for reasonable estimates of post-channeling enlargement by mass wasting and sapping processes, there may be much less disparity between source area and channel volumes than previously assumed in models for creating these channels by flood processes.

#### References Cited:

- Baker, V.R., and Kochel, R.C., 1979, *J. Geophys. Res.*, 84, p. 7961-7983.  
Carr, M.H., 1979, *J. Geophys. Res.* 84, p. 2995-3007.  
Chapman, M.G., and Scott, D.H., 1989, *Proc. 19th Lunar Planet Sci. Conf.*, p. 367-375.  
DeHon, R.A., 1989, *Abs. 20th Lunar Planet. Sci. Conf.*, p. 230-231.  
Grant, J.A., 1987, *NASA Tech. Mem.* 89871, p. 1-268.  
Kochel, R.C., and Burgess, C.M., 1983, *NASA Tech. Mem.* 85127, p. 288-290.  
Schumm, S.A., 1974, *Icarus*, 22, p. 371-384.

### Layered deposits with volcanic intrusions in Gangis Chasma, Mars.

G. Komatsu and R.G. Strom. Lunar and Planetary Laboratory, University of Arizona, Tucson, AZ 85721.

Layered terrains on the floor of Valles Marineris were first recognized in the Mariner 9 Images. They are about 100-200km long, 50km wide and 1-5km high, and characterized by well-developed, near-horizontal layers. Proposed origins are summarized by the following hypotheses:

1. Erosional remnants of the surrounding plains. This hypothesis is probably incorrect because the erosional style is very different than that of the canyon walls ([1],[2]). 2. Eolian deposits. Peterson [1] suggested that crossbedding in the Candor and Ophir layered terrains could be explained by global dust storm deposition, but Nedell, et al. [2] argued against this idea because of the lack of similar deposits on the surrounding plains and walls. 3. Pyroclastic deposits. A pyroclastic origin by ash fall or flow is based on the similarity between the erosional pattern of terrestrial ash flow and welded tuff and that of the resistant layer in the Hebes layered terrain [1]. However, because there are no similar deposits on the surrounding plains and no evidence for an associated caldera, Nedell, et al. [2] rejected this hypothesis. 4. Lacustrine deposits. This hypothesis is favored because it can explain the location, near horizontality, lateral continuity, great thickness and stratigraphic relationship ([2],[3],[4]). Moreover, a substantial subsurface aquifer system may have supplied water to fill or partially fill the canyons at or near the time of outflow channel and canyon formation [2].

Geologic setting of Gangis layered terrain. The area surrounding the Gangis layered terrain show a variety of geologic features relevant to its origin (Fig. 1). The canyon walls are about 2km high and show gully and spur topography and landslides. Fewer craters on the canyon floor than on the surrounding plains suggests that the floor is younger, possibly as a result of fluvial or eolian processes. A large crater on the southern upper plain shows evidence of ponding and outburst of water to the east forming an outflow channel. On the western part of the canyon floor are blocky mesas a few to 20km across and about 1km high. Their morphology is similar to the mesas of chaotic terrains thought to be the source of outflow channels. To the south and southeast of the layered terrain there are clusters of small hills 1-5km wide and a few hundreds of meters high. These may also be eroded remnants of chaotic terrain or they could be volcanic constructs. Their color is similar to the canyon floor.

Gangis layered terrain. The approximate size of Gangis layered terrain is 100km, 40-50km wide, and 1.5-2.0km high. To the west, the terrain seems to have been more eroded than to the east. The relatively gentle south-facing side has a slope of a few degrees, and is conspicuously fluted. This fluting could be due either to wind scouring or to the seepage of ground water. On the eastern part of the south-facing side are two blocky slabs, each about 10km wide. Their blocky nature and fold-like texture in them suggest they may be large landslide masses that have been subsequently shaped by erosion. Extending in a north-south direction from the summit of the layered terrain to near its base are several lines of darker domes and ridges. In some cases, areas of dark material surround the domes. These structures may be volcanic domes and dikes intruded into the layered deposits and subsequently exposed by the erosion which shaped the present-day layered terrain. The associated dark deposits could be erosional products from the structures or pyroclastic material. Part of slope has texture smoother than the fluted area. This region could be covered by the pyroclastic material suggesting volcanism could have been active until recently. The layered terrain itself can be divided into three main stratigraphic units (A,B,C in Fig.1) based on the erosional morphology. Each main unit consists of other less well-defined units not shown in Fig.1. The upper two layers are relatively thin and have steeper slopes than the lower unit. Strata within the middle unit(B) appear to thin and pinch out against the upper unit(C) suggesting an angular unconformity (arrow 1). Similarly, a dark layer within the lower unit (A) appears truncated by the middle unit indicating another angular unconformity (arrow 2). To the west, these three main units disconformably overlie a heavily eroded base rock that might be ancient cratered terrain. The angular conformities between the main stratigraphic units suggest that there were at least two intervals of erosion between the deposition of these three units. Domes, ridges and dark materials suggest that volcanism has modified the Gangis layered terrain. Whether Gangis layered terrain was laid down in a lake is still controversial, but assuming it originated as sedimentary deposits in the lake and the angular unconformities are real, then the following sequence of events appears to apply.

1. Formation of early closed Gangis Chasma and filling with water from subsurface. Hills and mesas may be remnants of chaotic terrain associated with this event. 2. Layer A deposited. 3. Draining or evaporation of lake and erosion of layer A during minor tectonic tilting. 4. Refilling of canyon with water from subsurface and deposition of layer B unconformably on layer A. 5. Draining or evaporation of lake and erosion of layer B during minor tectonic tilting. 6. Refilling of canyon with water from subsurface and deposition of layer C unconformably on layer B. 7. Intrusion of volcanics into layered deposits. 8. Catastrophic draining of lake to the east and erosion of layered deposits to expose volcanic intrusions.

Layered terrains may provide important clues for understanding the history of canyon formation and the Martian hydrologic cycle. Our current interpretation suggests multiple cycles of canyon filling and draining. This may be consistent with the proposed cycles of ancient oceans in the northern plains [5].

**REFERENCES** [1] Peterson, C. (1981). Proc. Lunar Planet. Sci. 12B, p.1459-1471. [2] Nedell, S.S., et al. (1987). Icarus, 70, 409-441. [3] Lucchitta, B.K. (1982). Report of Planetary Geology Program, p.233-234. NASA- TM 85127 [4] McCauley, J.F. (1978). Geologic map of the Coprates quadrangle of Mars. U.S. Geological Survey, Misc. Inv. Map I-897. [5] Baker, V.R., et al. (1990). Lunar and Planet. Sci. XXI.

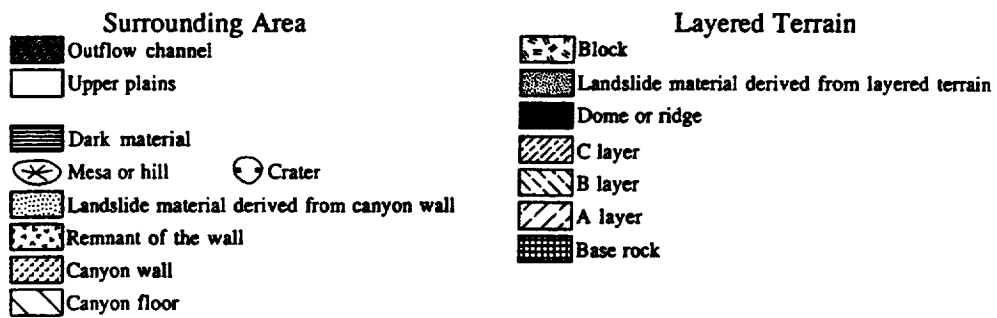
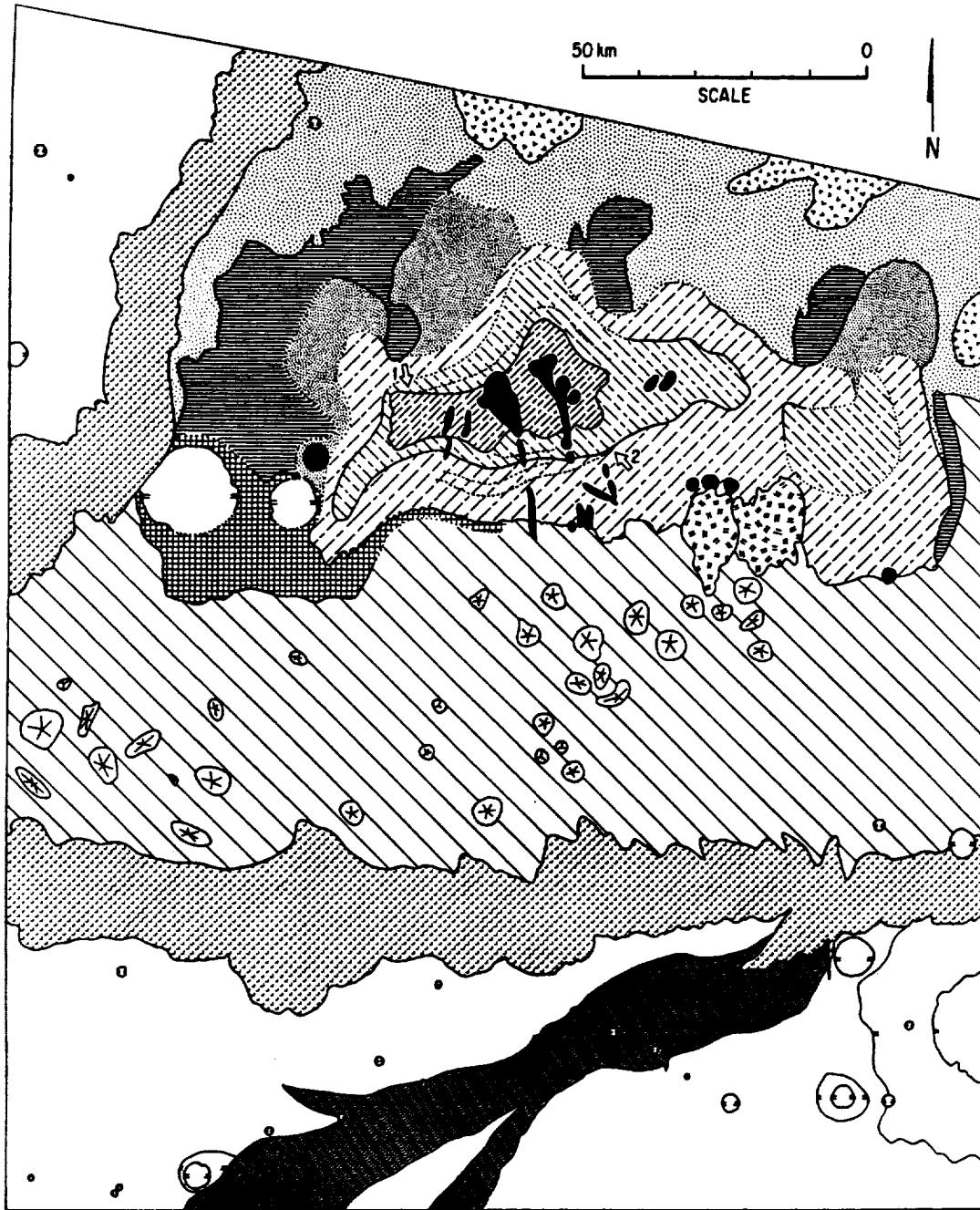


Figure 1. Geologic map of western Gangis Chasma.

VARIATION OF THE BOUND WATER CONTENTS ON THE MARTIAN SURFACE FROM  
ISM-EXPERIMENT DATA ON PHOBOS-2: PRELIMINARY RESULTS

R.D.Kuzmin, Vernadski Inst.USSR Academy of Sciences,Moscow 117975 USSR,V.I.Moroz, A.V.Grigoryev, Y.V.Nikolsky, N.F.San'ko, I.V.Khatuntsev, A.V.Kiselev.IKI USSR Academy of Sciences,Moscow 117485 USSR, J.P.Bibring, Y.Langevin, A.Soufflot.IAS/LPSP/University,Orsay,France, M.Combes.Observatoire de Meudon, France.

The spatial variations of the bound water in the martian soil were studied on the example of the fourth regions of the Mars:1-Melas and Ophir Chasmata ( $5-18^{\circ}\text{S}, 59-94^{\circ}\text{W}$ );2-Pavonis Mons ( $5^{\circ}\text{S}-3^{\circ}\text{N}, 95-126^{\circ}\text{W}$ );3-Ascraeus Mons ( $5.5-13^{\circ}\text{N}, 95-117^{\circ}\text{W}$ );4-Olympus Mons ( $12-18^{\circ}\text{N}, 112-146^{\circ}\text{W}$ ).The mapping of the bound water contents (in conventional values) was done using the spectral measurements in the absorption band  $2.7-3.14\mu\text{m}$  with the spatial resolution  $20 \times 30 \text{ km}$ [1].As turned out from all four regions the highest values of the bound water contents (or the hydration degree) were found in the Olympus Mons region - 23% more than those in the Melas and Ophir Chasmata.The hydration degree fluctuations in the martian soil within the studied regions are not identical and are estimated 26%,11%,6% and 9% for Regions 1,2,3,4 respectively.

Within each region the appreciable correlation between the spectral measurements in the band absorption by atmospheric  $\text{CO}_2$  (an equivalent of the altitudes) and mapped values of the soil hydration is not observed.However a certain tendency to clustering is visible.In each region the altitude range in which there is a certain range of the most widespread values of the bound water contents stands out (Fig.1).For Regions 1,2,3,4 such clusters values (into the contour 20 on Fig.1) are equal 35.2%,44.6%,27.8% and 56.7% of all the mapped values respectively.Using the new topographic map of the Mars[2],the mapped values of the spectral data for  $\text{CO}_2$  atmospheric abundance and bound water contents in the surface materials conform with all altitude range for four regions.As a result the united scale of the conventional values of the bound water contents was worked out and tied to the hypsometric scale of the Mars.

As demonstrated in Fig.2, a tendency to increasing of the clusters values of the hydration degree is observed in direction from the Region 1,through Region 2-3 to Region 4.Moreover,it was found that the clusters values are just on the shield surface only in the case of Pavonis Mons.In the other regions the clusters values of the hydration degree are usually on the surface around Ascraeus Mons,Olympus Mons and on the upper surface levels of Melas and Ophir Chasmata.It is typical that the successive increasing of the hydration degree of the soil from Region 2,through Region 3 to Region 4 is accompanied by the altitude fall of the terrain surface.Alternatively to such tendency,the dependence of the maximum values of the hydration degree from altitude is inversely (Fig.2).The region of Melas and Ophir Chasmata stands as exception.Here the lots of the higher hydration degree mostly relate to the sedimentary deposits (possibly lake-like deposits [3]), which filled the inner parts of Melas and Ophir Chasmata and its landslide slopes disposed on the lower hypsometric levels. Moreover,the clusters and the maximum values of the surface material hydration in the region of Ascraeus Mons are only on the shield surrounding surface, while the material directly on the shield surface is less hydrated. The fact,that the surface of this volcanic shield is covered by much coarser materials in comparison with the material of the surrounding plain[4] may be one of the reasons of such hydrated material distribution.

The visible tendency to the increasing of the surface material hydration from Region 1 to Region 2-4 is probably connected with the change (in the same direction) of the physical properties by surface material. For the surface material of Tharsis Montes area had lower thermal inertia values and lighter albedo [5], we believe that the weathering product portion in the surface material of Region 2-4 may be much higher than in Region 1.

On the whole it is not excluded that the found geographical and hypsometrical positions of the clusters and maximum values of the martian material hydration are defined by the possible dependence of the hydrated minerals phases on the geographical latitudinal (and altitudinal) zonality. In our case, the geographical latitude of the regions studied changes from  $18^{\circ}\text{S}$  to  $18^{\circ}\text{N}$  in direction from the first to the fourth regions. According to thermodynamic prediction of the stability of the salt hydrates in the modern environments of the Mars[6], increasingly hydrated phases must become more stable with latitude increase (example  $\text{MgCl}_2 \cdot \text{H}_2\text{O}$  on equator and  $\text{MgCl}_2 \cdot 4\text{H}_2\text{O}$  in moderate latitudes).Possibly the continuation of the more detailed analysis of the whole data from ISM-experiment may allow to examine the thermodynamic prediction.

REFERENCES:[1] Bibring J.P. et.al,Nature,1989,V.341,N 6243,p.591-593.[2] Atlas of Mars 1:15 000 000 Topographic series,M15M 0/90T,M15M 0/270,1988.[3] Nedell S.S. et.al,Isarus,1987,V.70,N 3,p.409-441.[4] Zimbelman J.R.,Greeley R.,3-d Int.Colloq.on Mars,1981,p.291-293.[5] Kieffer H.H. et.al, J.Geophys.Res.,1977,V.82,N 28, p.4249-4292.[6] Zolotov M.Yu.,LPSC,XX,1989,p.1257-1258.

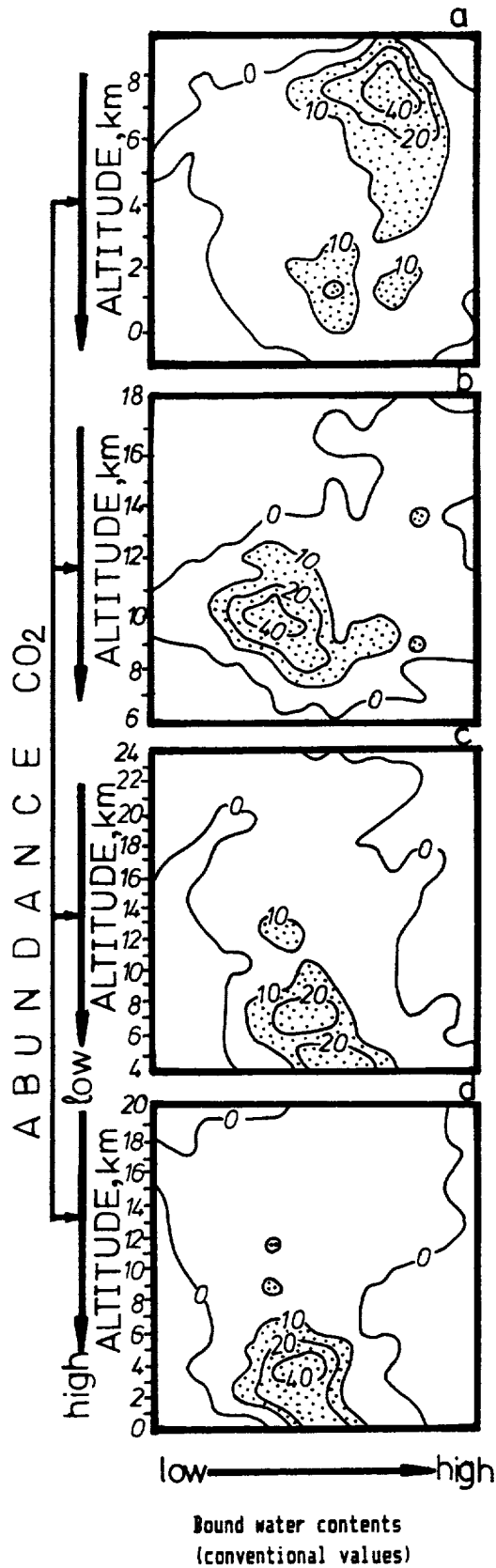


Fig.1. Spectral measurements of CO<sub>2</sub>-abundance in atmosphere versus the bound water contents (in conventional values) as a contour map. Regions: A-Melas and Ophir Chasmata; B-Pavonis Mons; C-Ascraeus Mons; D-Olympus Mons.

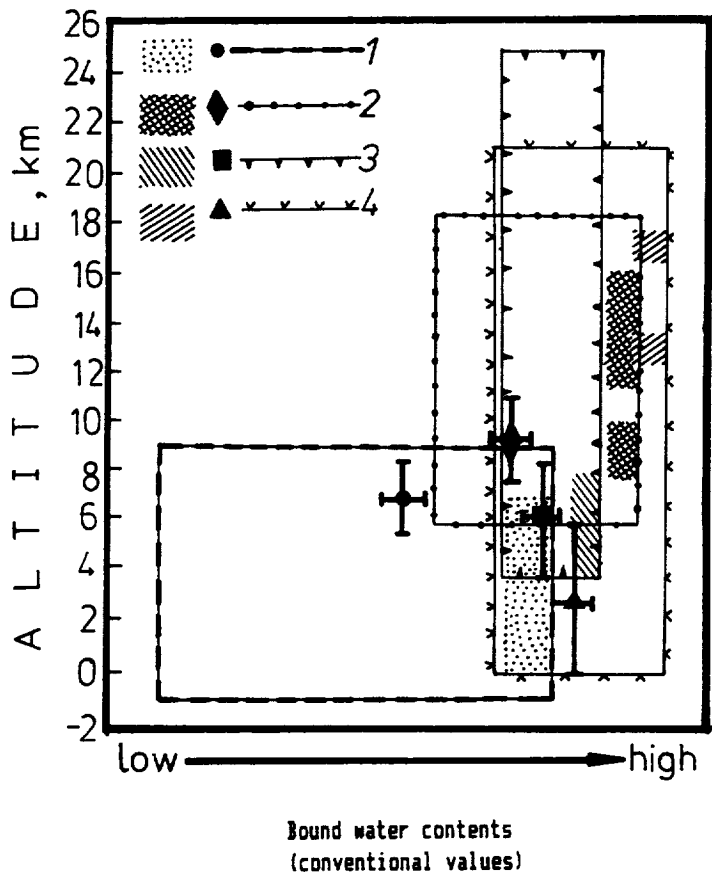


Fig.2. Altitude range of the regions studied (1,2,3,4) and corresponding clusters (symbols) and maximum (shaded areas) hydration values of the surface materials.

**THE EFFECTS OF ATMOSPHERIC DUST ON OBSERVATIONS OF THE SURFACE ALBEDO OF MARS; S.W. Lee and R.T. Clancy, Laboratory for Atmospheric and Space Physics, Univ. Colorado, Boulder, CO 80309**

The Mariner 9 and Viking missions provided abundant evidence that aeolian processes are active over much of the surface of Mars [1; 2]. Past studies have demonstrated that variations in regional albedo and wind streak patterns are indicative of sediment transport through a region [3; 4], while thermal inertia data [derived from the Viking Infrared Thermal Mapper (IRTM) data set] are indicative of the degree of surface mantling by dust deposits [5; 6; 7; 8; 9]. The visual and thermal data are therefore diagnostic of whether net erosion or deposition of dust-storm fallout is taking place currently and whether such processes have been active in a region over the long term. These previous investigations, however, have not attempted to correct for the effects of atmospheric dust loading on observations of the martian surface, so quantitative studies of current sediment transport rates have included large errors due to uncertainty in the magnitude of the "atmospheric contamination".

We have developed a radiative transfer model which allows the effects of atmospheric dust loading and variable surface albedo to be investigated [see related abstract, 10]. This model incorporates atmospheric dust opacity, the single scattering albedo and particle phase function of atmospheric dust, the bidirectional reflectance of the surface, and variable lighting and viewing geometry.

The Cerberus albedo feature has been examined in detail using this technique. Previous studies have shown the Cerberus region to have a moderately time-variable albedo [4]. IRTM observations obtained at ten different times (spanning one full martian year) have been corrected for the contribution of atmospheric dust in the following manner:

- A "slice" across the IRTM visual brightness observations was taken for each time step. Values within this area were binned to 1° latitude, longitude resolution.
- The atmospheric opacity ( $\tau$ ) for each time was estimated from [11]. As the value of  $\tau$  strongly influences the radiative transfer modelling results, spatial and temporal variability of  $\tau$  was included to generate an error estimate.
- The radiative transfer model was applied, including dust and surface phase functions, viewing and lighting geometry of the actual observations, and the range of  $\tau$  [10].
- Offsets were applied to the visual brightness observations to match the model results at each  $\tau$  (Figure 1).
- The "true surface albedo" was determined by applying the radiative transfer model to the offset brightness values, assuming  $\tau = 0$  and a fixed geometry (0° incidence, 30° emission). Repetition of this technique for each time step allows values of albedo for specific locations to be tracked as a function of time (Figure 2).

The initial results for Cerberus indicate the region darkens prior to the major 1977 dust storms, consistent with erosion of dust from the surface (possibly contributing to the increasing atmospheric dust load). There is some indication of regional brightening during the dust storms followed by a general darkening, consistent with enhanced dust deposition during the storms followed by erosion of the added dust. There is only minor variability during the second year, consistent with little regional dust transport during that period.

The results of this study indicate that atmospheric dust loading has a significant effect on observations of surface albedo, amounting to albedo corrections of as much as several tens of percent. This correction is not constant or linear, but depends upon surface albedo, viewing and lighting geometry, the dust and surface phase functions, and the atmospheric opacity. It is clear that the quantitative study of surface albedo, especially where small variations in observed albedo are important (such as photometric analyses), needs to account for the effects of atmospheric dust loading. Our future work will expand this study to other regional albedo features on Mars.

This research was supported under NASA Planetary Geology grant NAGW 1378.

**REFERENCES:** [1] Veverka, J., P. Thomas, and R. Greeley (1977). A study of variable features on Mars during the Viking primary mission. *J. Geophys. Res.* 82, 4167-4187. [2] Thomas, P., J. Veverka, S. Lee, and A. Bloom (1981). Classification of wind streaks on Mars. *Icarus* 45, 124-153. [3] Lee, S.W., P.C. Thomas, and J. Veverka (1982). Wind streaks in Tharsis and Elysium: Implications for sediment transport by slope winds. *J. Geophys. Res.* 87, 10025-10042. [4] Lee, S.W. (1986). Regional sources and sinks of dust on Mars: Viking observations of Cerberus, Solis Planum, and Syrtis Major (abstract), In *Symposium on Mars: Evolution of its Climate and Atmosphere* (V. Baker et al., eds.), pp. 71-72, LPI Tech. Rpt. 87-01, Lunar and Planetary Institute, Houston. [5] Kieffer, H.H., T.Z. Martin, A.R. Peterfreund, B.M. Jakosky, E.D. Miner and F.D. Palluconi (1977). Thermal and albedo mapping of Mars during the Viking primary mission. *J. Geophys. Res.* 82, 4249-4295. [6] Christensen, P.R. (1982). Martian dust mantling and surface composition: Interpretation of thermophysical properties. *J. Geophys. Res.* 87, 9985-9998. [7] Christensen, P.R. (1986). Regional dust deposits on Mars: Physical properties, age, and history. *J. Geophys. Res.* 91, 3533-3545. [8] Christensen, P.R. (1986). The distribution of rocks on Mars. *Icarus* 68, 217-238. [9] Jakosky, B.M. (1986). On the thermal properties of martian fines. *Icarus* 66, 117-124. [10] Clancy, R.T., and S.W. Lee (1990). Derivation of Mars atmospheric dust properties from radiative transfer analysis of Viking IRTM emission phase function sequences. *Reports of Planetary Geology and Geophysics Program*, this volume. [11] Martin, T.Z. (1986). Thermal infrared opacity of the Mars atmosphere. *Icarus* 66, 2-21.

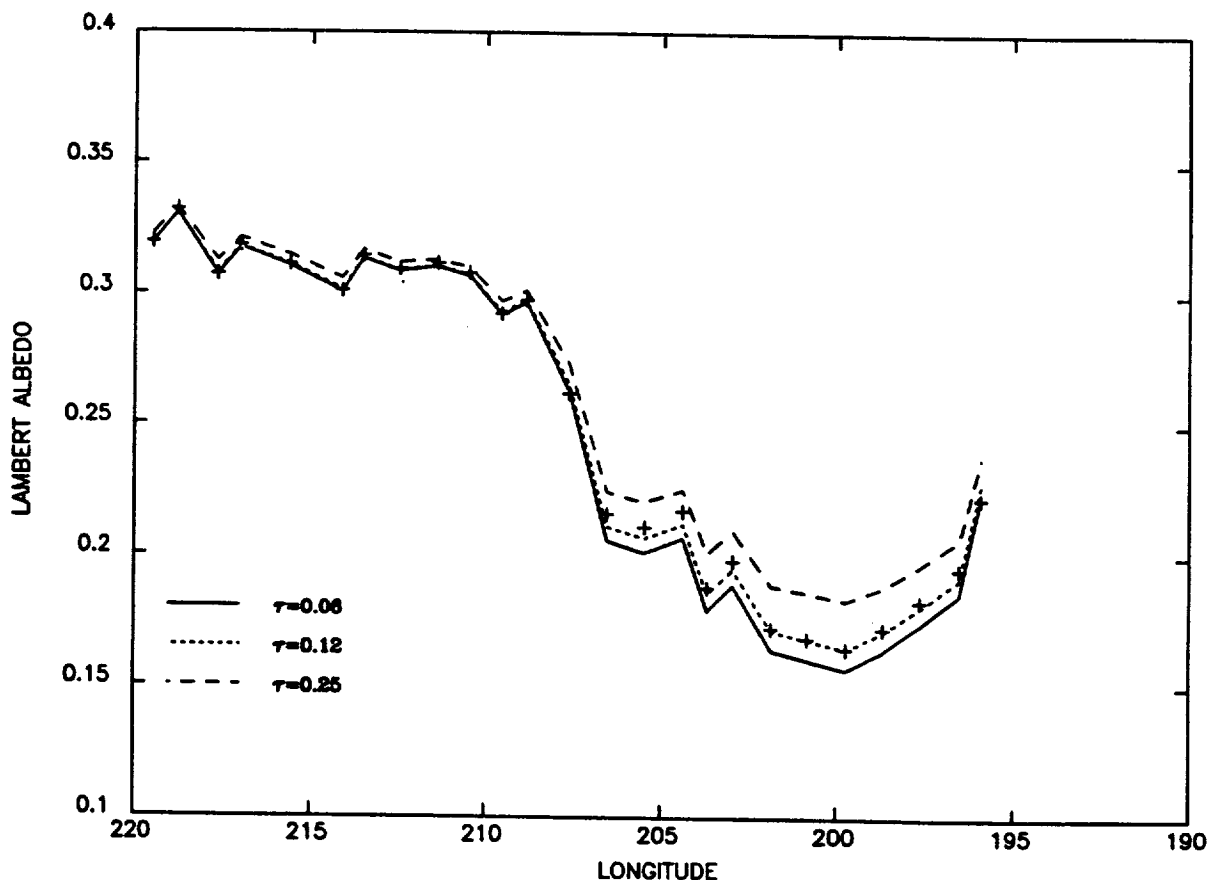


**Figure 1:** Results of the radiative transfer modelling for an albedo slice across Cerberus (latitude  $13^\circ - 14^\circ$ ) at  $L_s$   $124^\circ$ . Crosses indicate the actual observations, and lines denote the model results for three different opacities.

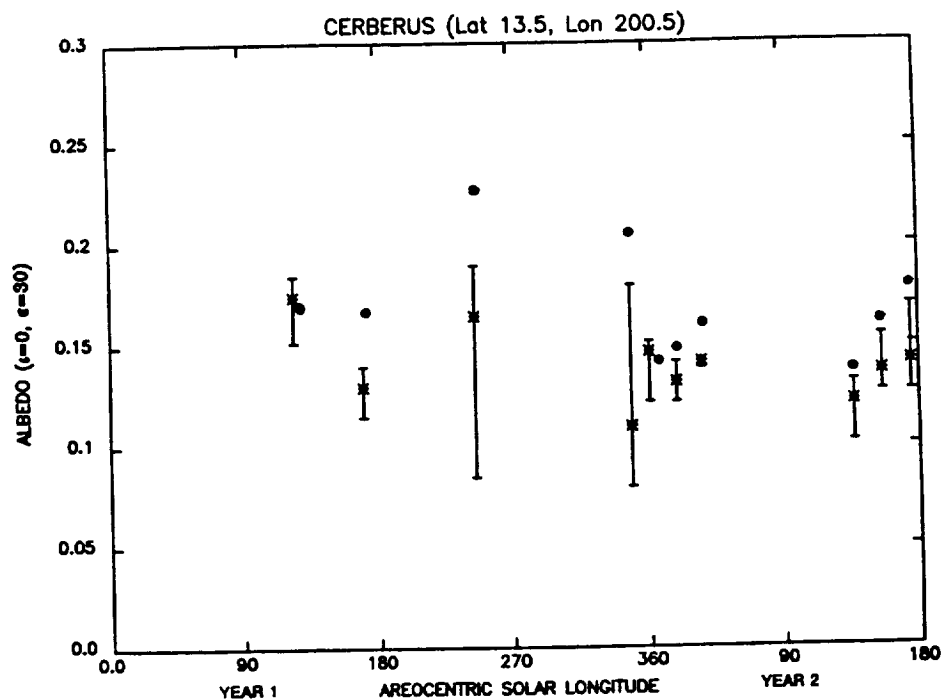


Figure 2a: Temporal behavior of a dark area in Cerberus. "True surface albedos" are denoted by asterisks; error bars indicate uncertainty in  $\tau$ . Uncorrected albedos are denoted by dots.

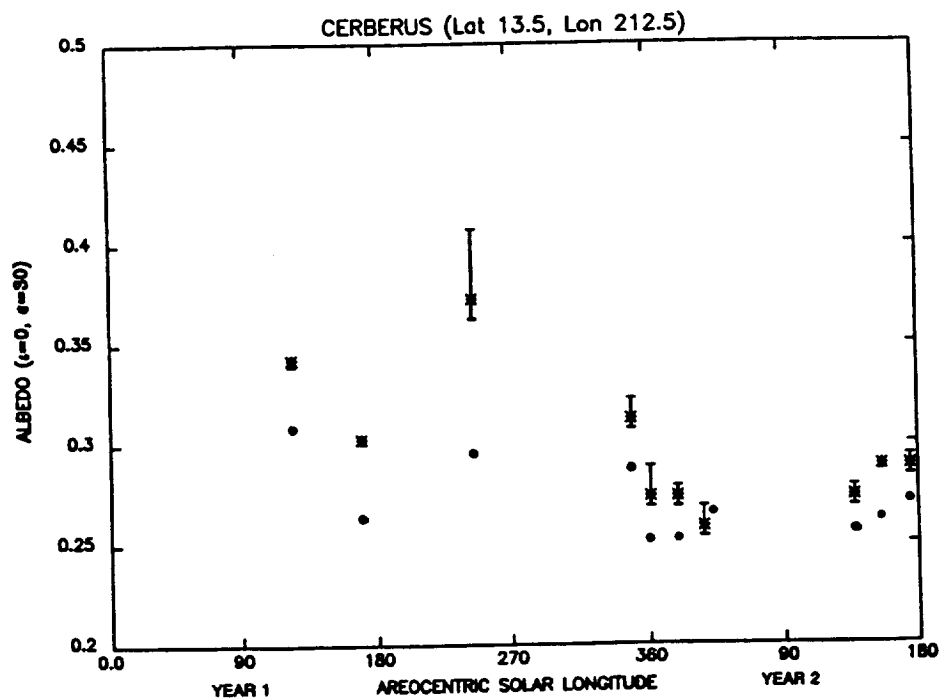


Figure 2b: Temporal behavior of a bright area in Cerberus. "True surface albedos" are denoted by asterisks; error bars indicate uncertainty in  $\tau$ . Uncorrected albedos are denoted by dots.